Structural elements in the oxidation process of a single cobalt layer on Ir(100)-(1 × 1)

Matthias Gubo, Christina Ebensperger, Wolfgang Meyer, Lutz Hammer, and Klaus Heinz
Lehrstuhl für Festkörperphysik, Universität Erlangen-Nürnberg, Staudtstrasse 7, D-91058 Erlangen, Germany
(Received 12 August 2010; revised manuscript received 20 December 2010; published 28 February 2011)

The ordered phases developing in sequence by oxidation of a single monolayer of cobalt deposited on Ir(100)-(1 × 1) were investigated by low-energy electron diffraction (LEED), scanning tunneling microscopy, and thermal desorption spectroscopy. It turns out that the structural elements of the different phases observed for increasing oxygen content and analyzed by quantitative LEED are pyramids based on squares or triangles made up by cobalt species and oxygen on top. The Co-O bond lengths are smaller than in the bulk of cobalt oxide owing to the reduced coordination of oxygen. For O:Co ratios of $r = 1/4$, $1/2$, and $5/8$, the bonding of the oxide to the iridium substrate is merely by the cobalt species, and at $r = 1$ it is via both Co and O.

DOI: 10.1103/PhysRevB.83.075435 PACS number(s): 68.47.Gh, 68.55.Nq, 68.90.+g, 61.05.jh

I. INTRODUCTION

Nanosized oxides promise to play an important role in the development of nanotechnologies with applications in, e.g., electronic and magnetic devices or chemical sensors. In particular, ultrathin oxide films with thicknesses of up to only a few oxide layers are most interesting as they exhibit new physical properties that do not apply to the related bulk oxides. These properties come, as well reviewed in recent papers,[1,2] by the hybrid character of such systems that is based on the interaction between the oxide layer(s) and the substrate. On the one hand, the substrate can strain the oxide layer (in the case of epitaxial growth) and, on the other hand, there is electronic interaction between the subsystems. Both the strain imposed and the electronic interaction depend on the stoichiometry of the oxide film that so adds an additional degree of complexity to the scenario.

In this paper we concentrate on the latter point and report on the structure of cobalt-oxide films epitaxially grown on the unreconstructed (100) surface of iridium, Ir(100)-(1 × 1). The oxygen content of a single cobalt oxide layer is varied assuming O:Co ratios of $r_{O:Co} = 1/4$, $1/2$, $5/8$, 1, and 2, whereby, respectively, superstructures of (2 × 2), $(3 \times 3)_I$, $(3 \times 3)_{II}$, $c(10 \times 2)$, and $c(8 \times 2)$ periodicity relative to the substrate unit-cell develop. Quantitative structural analyses of the $(3 \times 3)_{II}$ and $c(10 \times 2)$ phases were published recently,[3,4] so that in the present paper's emphasis is on the investigation of the other superstructures. We present structure determinations of the (2 × 2) and $(3 \times 3)_I$ phases and document the appearance of the $c(8 \times 2)$ superstructure. In order to describe the whole scenario consistently, we will recall the former results shortly and put them in context with the new structures. As earlier, atomically resolved scanning tunneling microscopy (STM) and quantitative low-energy electron diffraction (LEED) were applied to resolve the structures with crystallographic precision. Additionally, thermal desorption spectroscopy (TDS) was used to monitor the oxygen desorption from the different phases in order to relate their oxygen contents to each other and to get some idea about the bonding strength of oxygen.

In the following section we describe the preparation of the substrate and the oxidic films. Also, details about the LEED, STM, and TDS measurements as well as about the structural analysis of the LEED intensities are provided. In the third section we give a short survey of the different ordered phases that develop with increasing oxygen content. In the subsequent section we present the crystallography of the (2 × 2) and $(3 \times 3)_I$ phases as determined by STM and quantitative LEED. In the penultimate section we discuss the characteristic structural figures that develop with increasing oxygen content. The results are concluded in the final section.

II. EXPERIMENTAL AND COMPUTATIONAL DETAILS

The investigations were carried out in a two-stage ultrahigh vacuum apparatus with one vessel hosting a homemade three-grid LEED optics, a quadrupole mass spectrometer for TDS, and an electron-beam-operated evaporator for highly purified cobalt and the other a commercial beetle-type STM as described earlier.[5] There was easy transfer between the two stages. The unreconstructed but metastable (100) surface of iridium, Ir(100)-(1 × 1), was prepared from the stable and hexagonally reconstructed surface. This was accomplished by oxygen-induced lifting of the reconstruction followed by the removal of oxygen via hydrogen exposure.[6–8] The oxide films were prepared by deposition of slightly less than a monolayer (ML) of cobalt on the clean substrate (in the following, 1 ML is regarded to have the same atomic density as the substrate layers). This was followed by exposure to an oxygen atmosphere of $\sim 5 \times 10^{-9}$, mbar estimated at the position of the sample whose temperature was held at 50 °C. Exposure for ∼1 min produced a (2 × 2) superstructure pattern in LEED. After additional exposure for 2 min, the first (3 × 3)-periodic superstructure developed, $(3 \times 3)_I$. Continued exposure by another 3 min triggers the continuous transition to a second structure of this periodicity, $(3 \times 3)_{II}$. By heating to ∼250 °C and additional exposure to 5×10^{-8} mbar oxygen for 2 min followed by a flash to 400 °C, the $c(10 \times 2)$ superstructure appears. When the cobalt layer is exposed to oxygen at liquid-nitrogen temperature and the system subsequently annealed at 400 °C, the $c(8 \times 2)$ phase appears. It can be prepared also by reactive deposition of Co in an oxygen atmosphere of as high as $\sim 10^{-6}$ mbar and at an elevated sample temperature of ∼250 °C.

STM images were taken at room temperature whereby atomic resolution could be achieved for (positive) tip voltages in the range up to 0.5 V. For the structure analysis, LEED patterns and intensity versus energy spectra, $I(E)$, were

recorded for normal incidence of the primary beam with the sample at liquid-nitrogen temperature and using a computer-controlled video method.[9] Symmetrically equivalent spectra were averaged. The total database in each case was maximized by collecting data in the energy range 40–600 V. For the TDS measurements a linear increase of the temperature with time (7 K/s) was applied for which the signal of desorbing oxygen in the quadrupole mass spectrometer was measured. The latter was provided with a cup close to the surface and differentially pumped from the rear, so that only oxygen desorbing from the sample entered the spectrometer.

The crystallographic structures of the (2×2) and $(3 \times 3)_{\mathrm{I}}$ phases from the measured $I(E)$ spectra were revealed by use of the perturbation method TENSORLEED,[9–11] applying the TENSERLEED code.[12] The structural search was realized by a frustrated simulated annealing procedure[13] controlled by the Pendry R-factor[14] to compare experimental and simulated spectra on a quantitative scale. A maximum of 14 phase shifts were used, calculated as described in Ref. 15. They were corrected for isotropic thermal vibrations at the temperature of measurement (100 K) with the vibrational amplitudes as additional fitting parameters. Electron attenuation was simulated as usual by an optical potential, which was determined as $V_{0i} = 6$ eV. The real part of the inner potential was taken to be energy dependent according to Ref. 15 in order to account for the energy dependence of the exchange-correlation potential. The statistical error limits for the model parameters determined were estimated by applying the variance of the R-factor, $\mathrm{var}(R) = R\sqrt{8V_{0i}/\Delta E}$,[14] whereby, however, parameter correlations were neglected. For the vertical atomic coordinates the errors amount to ~0.02–0.04 Å for Co and Ir and up 0.06 for O. The errors for lateral coordinates are up to 0.05 Å for Co and up to 0.07 Å for O.

III. SURVEY OF THE DIFFERENT PHASES

Figure 1 gives a survey of the LEED patterns of the different phases developing with increasing O:Co ratio. The (noncentered) reciprocal unit cell is inserted in each case. The sharpness of the spots indicates that all superstructures are well ordered. Figure 1(d) displays the spectra of the same beam for the two (3×3) phases. The drastic differences prove that indeed they must be two different structures. Each spectrum exhibits minima with vanishing intensity at positions where the other spectrum shows high intensities. This is a safe indication that the structures can be (and are) prepared as single phases.

Heating of the oxide films up to 1200 °C causes the oxide to break up and the oxygen to desorb (while cobalt dissolves into the bulk of the iridium substrate). The corresponding TD spectra are displayed in Fig. 2(a). In the first place they were integrated to allow for the determination of the oxygen content of the different phases relative to each other, as given in Fig. 2(b). In order to retrieve the oxygen amount at an absolute measure, the data were calibrated using the results of recent quantitative LEED structure analyses, which proved the existence of 0.9 ML of oxygen with a ratio $r_{\mathrm{O:Co}} = 1$ for the $c(10 \times 2)$ phase[4] and 5/9 ML of oxygen with a ratio $r_{\mathrm{O:Co}} = 5/8$ for the $(3\times3)_{\mathrm{II}}$ phase.[3] They are shown as full circles and the straight line is the best-fit linear curve. From the integrated TD signal of the other phases (open circles), their

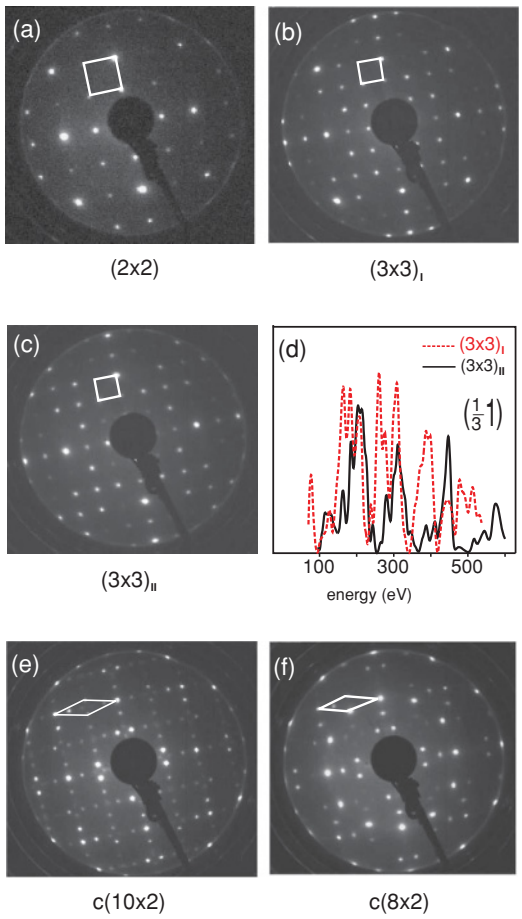

FIG. 1. (Color online) LEED patterns of the various phases at the same electron energy (100 eV). The reciprocal (noncentered) unit cell is inserted in each case. (d) compares the spectra of the $(\frac{1}{3}1)$ beam of the two (3×3)-periodic phases.

oxygen content is estimated using this line, yielding 0.21 ML for the (2×2) phase, 0.37 ML for $(3 \times 3)_{\mathrm{I}}$, and 1.77 ML for the $c(8 \times 2)$ structure. The spectral information given in Fig. 2(a) will be evaluated in the next section for the (2×2) phase, and information for the other phases will be addressed in the discussion.

IV. THE PHASES (2 × 2), (3 × 3)$_{\mathrm{I}}$ AND c(8 × 2)

Deposition of ~1 ML Co on Ir(100)-(1×1) results in a pseudomorphic epitaxial (1×1)-periodic cobalt layer, as displayed in the ball model of Fig. 3(a). The quantitative LEED intensity analysis ($R = 0.114$, $\Delta E = 2800$ eV) shows that the cobalt atoms reside in hollow positions of the iridium substrate (details of the analysis will not be given here in order to shorten the paper). The adlayer's position is 1.66 Å above the substrate. This is equivalent to a Co-Ir bond length of 2.54 Å, which, with an iridium radius of 1.36 Å, gives a cobalt radius of 1.18 Å. This is less than the value in the cobalt bulk, which is 1.25 Å (with respect to the latter, the Co-Ir layer spacing is contracted by 6%). The first layer spacing in the iridium substrate is 1.96 Å, slightly above the bulk value (1.92 Å), but significantly expanded compared to the value of the clean (1×1) surface [1.85 Å (Ref. 16)]. So the heteroepitaxial system Co/Ir(100)

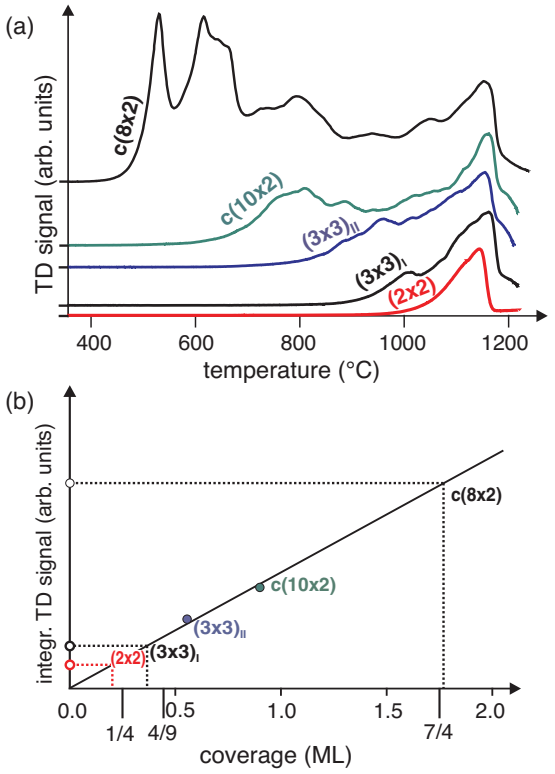

FIG. 2. (Color online) (a) TD spectra recorded for oxygen desorption from the different phases. Note that the data are ofset with respect to each other (as indicated at the ordinate) in order to avoid mutual overlap. In (b) the data of the integrated TD signal (background corrected) are presented as a function of coverage (see text).

fits to the usual surface relaxation pattern of fcc (100) surfaces, i.e., contraction of the first and expansion of the second layer spacing.

A. Crystallographic structure and bonding of the (2 × 2) phase

Exposure of the cobalt adlayer to oxygen first produces a (2 × 2) superstructure in LEED, in agreement with the STM image displayed in Fig. 3(b). In the LEED analysis the spectra of 25 symmetrically inequivalent beams (eight of integer and 15 of fractional order) with an accumulated total energy database width of $\Delta E = 8000$ eV were evaluated. In the structural search, in which fourfold rotational symmetry of the unit cell was assumed always, a best-fit R-factor of $R = 0.117$ was achieved (0.107 for the integer and 0.123 for the fractional order spots). The R-factor variance amounts to var(R) = 0.009. Figure 3(e) displays the quality of the theory-experiment fit visually for a selected beam.

In the best-fit model oxygen occupies every fourth hollow site of the cobalt layer, as displayed in Fig. 3(c). The corresponding oxygen coverage of nominally $\theta^{O}_{2\times2} = 1/4$ is consistent with the value obtained by TDS (0.21), given that not all sites formed by Co are occupied as outlined at the end of this paragraph (local Co coverage: $\theta^{Co}_{2\times2} = 1$). Oxygen attracts the surrounding cobalt species so that the latter move diagonally toward the oxygen. According to the LEED fit, this movement amounts to 0.13 Å [0.09 Å horizontally, see Fig. 3(c)]. Also,

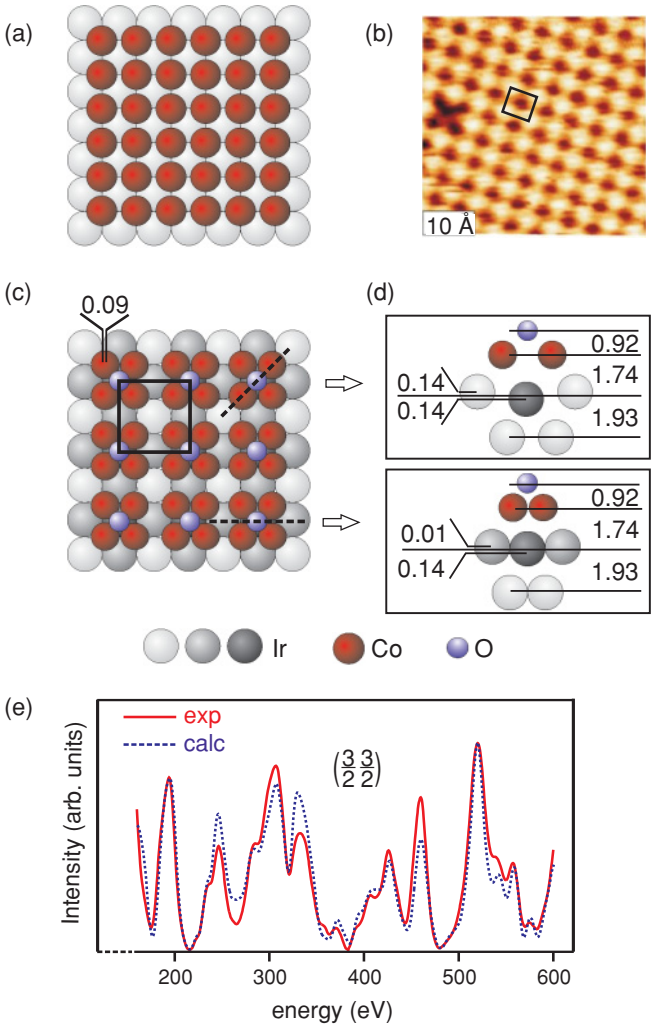

FIG. 3. (Color online) (a) Ball model of a single monolayer of cobalt deposited on Ir(100)-(1 × 1). (b) STM image (+0.42 V, 0.40 nA) of the cobalt layer after exposure to oxygen, exhibiting a (2 × 2) superstructure (the unit cell is inserted). (c) displays the ball model of the (2 × 2) phase in the top view. The related side views are given in (d) along the cuts indicated in (c), whereby the lower side view displays also the cobalt atoms projected on the cutting plane. The parameter values inserted are in Å units. (e) compares the experimental and best-fit calculated spectra for a selected beam (single-beam R-factor: $R = 0.093$).

there is a (repulsive) interaction of oxygen with the iridium atom directly below it so that the top iridium layer becomes buckled. This is indicated by the shading of atoms in Fig. 3(c) and quantitatively given in the diagonal and horizontal cuts vertical to the surface displayed in the two frames of Fig. 3(d). So the oxygen layer has imprinted its (2 × 2) superstructure also on the cobalt and top iridium layer. The vertical spacing between the cobalt layer and the center-of-position plane of the top iridium is increased to 1.74 Å (compared to the value of 1.66 Å for the bare cobalt layer). From the determined atomic coordinates, the Co-Ir and Co-O bond lengths can be calculated, 2.59 and 2.60 Å (for the inequivalent Ir atoms) and 2.02 Å, respectively. The (isotropic) vibrational amplitudes are 0.13 and 0.09 Å for the O and Co species, respectively. One should also note that in the STM image [Fig. 3(b)] the

oxygen species show up. This can be concluded from the single defect, i.e., missing bright ball. which—as it fits to a (2×2)-sized arrangement of surface protrusions—must be an oxygen species. Missing oxygen species lead to a reduced total oxygen coverage as observed in TDS.

The TD spectrum from the (2×2) phase is the simplest among the different spectra presented in Fig. 2(a) with a single peak at high temperature ($\approx$1150 °C). This is indicative for a single type of bonding environment of oxygen, as in fact was shown above. From the peak temperature T_m and assuming second-order desorption (although the peak shape is not strictly symmetric), one can estimate the binding energy E_b by the relation $E_b/kT_m^2 = \nu\theta_0\beta^{-1}\exp(-E_b/kT_m)$, whereby ν is the escape attempt frequency, β is the heating rate, θ_0 is the initial oxygen coverage, and k is the Boltzmann constant.[17] With $\nu \approx 10^{12}$ s^{-1}, $\beta = 7$ K/s, and $\theta_0 = 1/4$, a value of $E_b \approx 3$ eV results.

B. Crystallography and growth of the $(3 \times 3)_{\mathrm{I}}$ phase

As already described in Sec. II, further exposure of the (2×2) phase to oxygen leads to the $(3 \times 3)_{\mathrm{I}}$ superstructure. Its STM image is displayed in Fig. 4(a) with the unit cell inserted. In the LEED intensity analysis, spectra of 45 symmetrically inequivalent beams (eight of integer and 37 of fractional order) were evaluated whose accumulated energy database amounts to $\Delta E = 16\,200$ eV. The structural search procedure followed the same strategy as described for the $(3 \times 3)_{\mathrm{II}}$ phase (see Ref. 3) and assuming fourfold rotational symmetry of the unit cell. Again, it resulted in an excellent quality for the theory-experiment fit mirrored by an R-factor $R = 0.141$ (0.141 for the integer order and 0.142 for the fractional order beams) with a variance of var$(R) = 0.008$. A total of 22 structural parameters, including those for the first three Ir layers, were determined. Additionally, the vibrational amplitudes of the oxygen and cobalt species were varied. The large database allows the safe determination of so many parameters as the redundancy factor is as high as $\Delta E/4nV_{0i} \approx 28$ ($n = 24$ is the total number of parameters involved). For visual comparison of experimental and computed best-fit spectra, Fig. 4(b) presents the data for a selected beam.

The resulting best-fit structure is illustrated by ball models in top and side views in Figs. 4(c)–4(e). As evident from the large-scale top view in Fig. 4(c), the former arrangement of the (2×2) cobalt layer is drastically modified. One out of nine cobalt species is now missing, so that the (3×3) unit cell contains only eight Co (local Co coverage $\theta^{\mathrm{Co}}_{3\times3_{\mathrm{I}}} = 8/9$). Figure 4(d) shows that the Co species surrounding the vacancy relax toward it by as much as 0.47 Å (measured with respect to their original hollow sites on the iridium substrate). So, within the unit cell, four threefold coordinated hollow sites for oxygen are formed. They are indeed occupied by oxygen while the fourfold sites centered at the corners of the unit cell remain free. The nominal oxygen content is $\theta^{\mathrm{O}}_{3\times3_{\mathrm{I}}} = 4/9$, which is again consistent with the experimental value (0.37) given that there are defects and/or uncovered small surface patches. The stoichiometry of this $(3 \times 3)_{\mathrm{I}}$ phase is $r_{\mathrm{O:Co}} = 1/2$. As the Co species forming the fourfold site are shifted toward the oxygen by only 0.07 Å, the cobalt layer is buckled by an amplitude of 0.20 Å [see cut B in Fig. 4(e)]. This induces a buckling

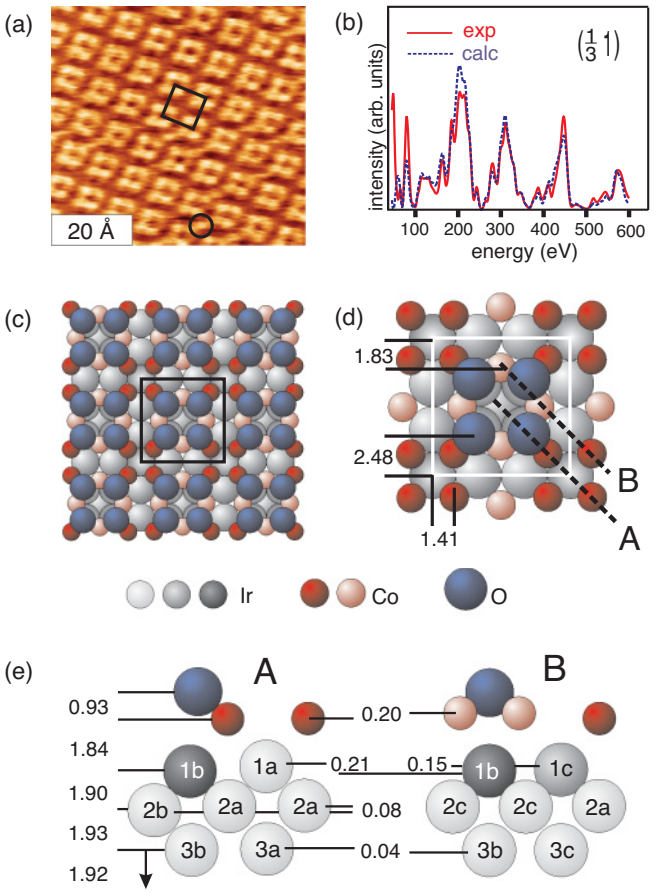

FIG. 4. (Color online) (a) STM image of the $(3 \times 3)_{\mathrm{I}}$ phase (+20 mV, 0.80 nA) with the unit cell inserted (the structural element encircled is commented on more below). (b) compares the experimental and best-fit calculated spectra for a selected beam (the single-beam R-factor is $R = 0.191$). The following panels display ball models in top views at different scales (c), (d) and side views (e) along the vertical planes A and B indicated in (d). The parameter values inserted are in Å units.

of the same order in the top iridium layer and even, although with a quickly vanishing amplitude, also on the second and third iridium layer. The spacing between the center-of-position planes of the top iridium layer and the cobalt layer is 1.84 Å, i.e., further increased as compared to the (2×2) phase (1.74 Å) owing to the larger shifts out of the hollow sites. In contrast, the spacing between the oxygen and cobalt layer is almost the same (0.93 Å vs 0.92 Å). The Ir-Co bond lengths calculated from the structural parameters are 2.57 and 2.59 Å and the Co-O bond lengths are 1.83 and 1.91 Å for the lower and higher lying Co, respectively. The vibrational amplitudes are 0.15 Å for O and 0.11 Å for Co.

The question arises as to where the Co species missing in the $(3 \times 3)_{\mathrm{I}}$ phase go when the transition $(2 \times 2) \rightarrow (3 \times 3)_{\mathrm{I}}$ takes place by extended exposure to oxygen. Related to that, we recall that in the first step of the oxide preparation, slightly less than a monolayer of cobalt had been deposited on the substrate. As has been observed by STM, it forms large (1×1) islands with correspondingly small uncovered areas in between, so that the $(3 \times 3)_{\mathrm{I}}$ phase can extend to the latter. To check for that scenario we prepared in an additional experiment a Co

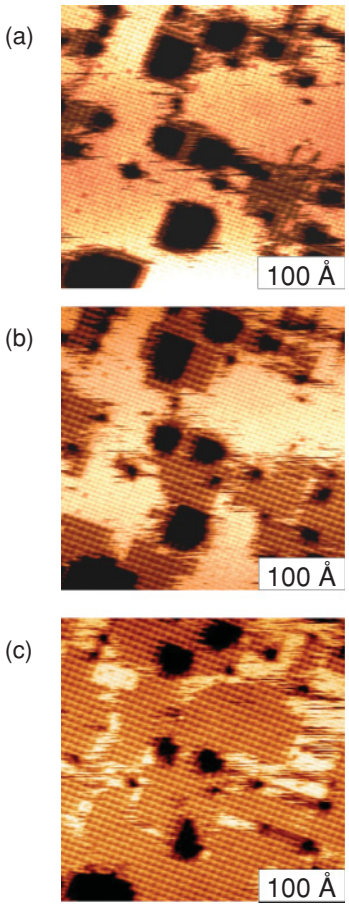

FIG. 5. (Color online) STM images for the very same surface area taken during oxygen exposure of an incomplete cobalt monolayer on Ir(100) at room temperature (+0.3 V, 0.4 nA). For details, see the text.

layer with significantly less than 1 ML coverage. Exposure to oxygen as described above again first produces the (2 × 2) phase with, however, a number of empty areas between its domains. This is presented in Fig. 5(a), whereby the bright areas correspond to (2 × 2) domains [identifiable by the (2 × 2) atomic grid]. The black areas represent uncovered surface patches. There are also some small ordered $(3 \times 3)_{\mathrm{I}}$ domains showing up as darker areas with a wider atomic grid. By further exposure to oxygen, the $(3 \times 3)_{\mathrm{I}}$ phase proceeds to grow [Figs. 5(b) and 5(c)] whereby the sizes of the uncovered domains shrink. This shows that the Co species removed from the $c(2 \times 2)$ phase are used to form additional parts of $(3 \times 3)_{\mathrm{I}}$ domains. Seemingly, the activation barrier for this process is low enough so that it can take place even around room temperature.

C. Information about the $c(8 \times 2)$ phase

As shown by the integrated TD signal [Fig. 2(b)], the $c(8 \times 2)$ phase contains nearly twice as much oxygen than the $c(10 \times 2)$ phase, which is of 1:1 stoichiometry as proven by quantitative structural analysis.[4] Figure 6 displays the STM image recorded for the $c(8 \times 2)$ phase with the (noncentered) unit cell inserted. It clearly shows a hexagonal arrangement of surface protrusions (seven per unit cell), which, however, is vertically modulated with a small buckling amplitude (0.1 Å)

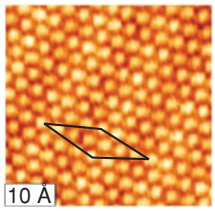

FIG. 6. (Color online) STM image of the $c(8 \times 2)$ phase (+2.2 mV, 0.43 nA) with the unit cell inserted.

in the direction parallel to the close-packed rows. The close packing is indicative for the presence of layers as in rocksalt-type CoO(111). In fact, the (average) lateral spacing of the protrusions within a row is $8a_{\mathrm{Ir}}/7 = 3.10$ Å, which is close to the spacing in CoO(111) (3.01 Å). The distance to the species in neighbored rows is 3.13 Å, so that the in-plane arrangement is almost ideally hexagonal. The STM appearance of the phase is similar to that observed for thicker CoO(111) films grown on Ir(100)-(1 × 1).[18] From the LEED unit cell and STM, the Co coverage is calculated to be $\theta^{\mathrm{Co}}_{c(8\times2)} = 7/8$, and with the knowledge that the oxygen content amounts to almost 2 ML [Fig. 2(b)], $\theta^{\mathrm{O}}_{c(8\times2)} = 7/4$ results. Accordingly, a CoO(111)-type O-Co-O trilayer model for the $c(8 \times 2)$ would be consistent with our data.

V. DISCUSSION

In the following section we discuss the structural elements of the newly quantitatively determined structures. In order to extend the view, we include also the already known phases, $(3 \times 3)_{\mathrm{II}}$ and $c(10 \times 2)$, in that discussion.

A. (2 × 2) phase

The structural element characterizing the (2 × 2) phase is a Co_4O pyramid with a square arrangement of Co species as the base and O on top [Fig. 7(a)]. On first glance, the structure resembles more a (2 × 2) oxygen adsorption system on the cobalt layer than a cobalt-oxide layer. Indeed, there is no bulk cobalt oxide with this oxygen-cobalt coordination observed. Also, for the formation of a rocksalt-type CoO(100) layer, in which the Co and O species are in the same plane with an in-plane lattice parameter of 3.01 Å, the spacing of the cobalt atoms on Ir(100) is much too small (2.72 Å). Even more, the oxygen residing in fourfold hollow position of the cobalt species attracts the latter so that their lateral spacing becomes even more reduced, i.e., 2.54 Å and so close to the hard sphere diameter in the Co bulk (2.51 Å).

The Co-O bond length of the fourfold coordinated oxygen in the (2 × 2) phase results to be 2.02 Å. Reasonably this is larger than the value of 1.85 Å determined in oxygen-terminated CoO(111) (Ref. 19) films or 1.83 Å for oxygen on $Co(10\bar{1}0)$ (Ref. 20) in which systems' oxygen is only threefold coordinated to cobalt. Also reasonably, it is smaller than the value of 2.13 Å in bulk rocksalt-type CoO, where oxygen is in octahedral sites with sixfold coordination to cobalt species (and Co sixfold coordinated to O). The single-peak oxygen TD spectrum from the (2 × 2) phase is in line with the fact that there is only one oxygen site involved and that there is no reordering of the Co species when oxygen species desorb.

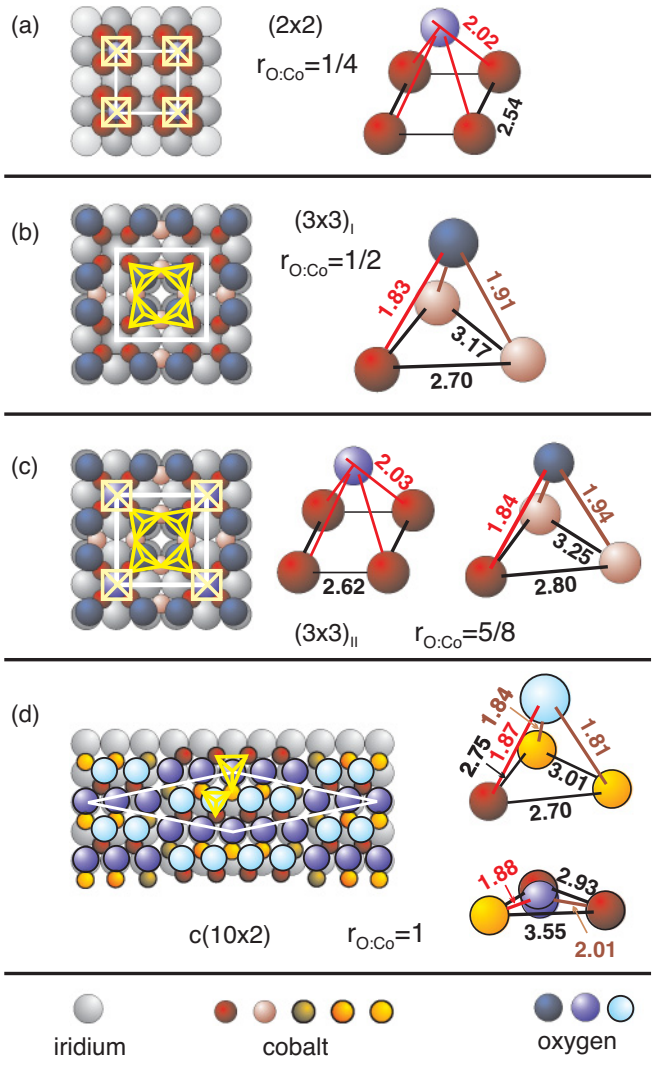

FIG. 7. (Color online) Top-view ball models of the quantitatively determined single-layer cobalt oxides (left-hand side) with their characteristic structural elements (right-hand side). The bond lengths given are in Å units.

B. $(3 \times 3)_I$ phase

In the next step of oxidation the $(3 \times 3)_I$ phase is produced. The coordination of oxygen to cobalt changes from fourfold to threefold. This is enabled by Co vacancy formation and subsequent local rearrangement of the surrounding cobalt species. So, as illustrated in Fig. 7(b), the oxidic structural element of this phase is a Co_3O pyramid formed by a Co triangle as the base with oxygen on top. Yet fourfold coordinated sites still remain, which, however, are not occupied. As a consequence, the corresponding Co species are no more shifted toward the center of the square as in the (2×2) phase but, in contrast, off this center because each of them belongs also to the species forming the threefold site. Quantitatively, the length of the square is expanded by 0.28 Å as compared to the (2×2) phase. Because of the vacancy, the actual stoichiometry, $r_{O:Co} = 1/2$, is not only owing to the increased density of oxygen (per substrate unit cell: $\theta^{O}_{2\times2} = 1/4 \rightarrow \theta^{O}_{(3\times3)_I} = 4/9$) but also owing to the decreased density of cobalt (per substrate unit cell: $\theta^{Co}_{2\times2} = 1 \rightarrow \theta^{Co}_{(3\times3)_I} = 8/9$).

There are different Co-O bond lengths in the Co_3O pyramid: The smaller one (1.83 Å) involves Co species forming the unoccupied square that do not share bonds with another oxygen and so can realize a stronger bond. The bond with the larger length (1.91 Å) involves Co species that bind to an additional oxygen. The existence of two types of Co species leads to a considerable buckling of the Co layer (amplitude 0.20 Å) and this distortion extends down to the third Ir layer. This deep-going reaction of the Ir substrate is not unusual and has also been observed for the stable phase of the clean substrate, Ir(100)-(5×1)-hex, whose top layer is quasihexagonally reconstructed.[16]

The pyramidal structural element locally resembles that in an oxygen-terminated rocksalt-type CoO(111) surface. Yet it is considerably distorted by the buckling of the cobalt layer and the lateral arrangement of the cobalt species: Those of the latter forming the threefold sites are not within a surface-parallel plane and do not form a regular triangle (their interatomic spacings amount to 2.70 and 3.17 Å). Also, the oxygen species on this site is not exactly on top of the next layer Ir atom (although it is near that position). Reasonably, both Co-O bond lengths are again shorter than that in the bulk of rocksalt-type CoO (2.13 Å). Also, reasonably, they are close to the values given above for oxygen in threefold coordination to Co.

The oxygen TD spectrum from the $(3 \times 3)_I$ phase exhibits a desorption peak at or near the same location as the (2×2) phase but also one at a lower temperature ($\approx$1000 °C). We propose that this is owing to the desorption of oxygen from the Co_3O pyramid. The lower binding energy appears to be reasonable owing to the reduced coordination of oxygen to cobalt. Yet obviously only few oxygen species desorb from the threefold site, which we interpret as owing to local reordering processes taking place when the Co_3O pyramid is broken. Assuming that such processes are reverse to those taking place when going from the (2×2) to the $(3 \times 3)_I$ phase, again Co_4O pyramids should develop from which oxygen desorbs only at higher temperatures as in the pure (2×2) phase. We also mention that the fact that the (2×2) phase appears to be rather stable tells us nothing about the activation barrier for the transition to the $(3 \times 3)_I$ phase. Also, different from the TDS experiments, this process proceeds under oxygen exposure. Moreover, as in the $(3 \times 3)_I$ phase, twice as many oxygen species are accommodated as compared to the (2×2) phase, and the large binding energy of oxygen provides substantial excess energy to overcome the activation barrier.

C. $(3 \times 3)_{II}$ phase

In the next ordered phase, $(3 \times 3)_{II}$, the arrangement of the cobalt species remains roughly the same, as has been analyzed recently (local coverages $\theta^{O}_{(3\times3)_{II}} = 5/9$, $\theta^{Co}_{(3\times3)_{II}} = 8/9$).[3] Yet now the fourfold sites are also occupied by oxygen, as illustrated in Fig. 7(c). This site occupation proceeds in a rather statistical way, as is obvious from the continuous transition of the LEED spectra as well as from the STM images. Some fourfold sites occupied already in the $(3 \times 3)_I$ phase can be identified in Fig. 4(a) as single protrusions between the squares of oxygen species (one of which is encircled). The Co forming

the fourfold site are shifted back toward their center so that the length of the square (2.62 Å) is again reduced with respect to the spacing between the iridium hollow sites (2.72 Å). Reasonably, this is less pronounced than in the (2 × 2) phase (2.54 Å) as the Co is also part of the occupied threefold site. The lengths of the triangle sides change accordingly. On the other hand, the Co-O bond lengths in both sites remain largely unchanged.

Desorption from the $(3 \times 3)_{II}$ starts at even lower temperatures. This is in qualitative agreement with the fact that, in this phase, the Co species of the now occupied fourfold adsorption sites also bind to another O species, reducing the binding energy of this site as compared to the (2 × 2) phase. Vice versa, the oxygen bonding in the Co_3O pyramid is also weakened, so that it can hardly be judged as to which of the different oxygen species in the structure would desorb first. Because the desorption process cannot be monitored by LEED owing to the very high temperatures involved, it is even unclear so far, whether the desorption proceeds from the ordered state at all or from a thermally disordered one.

D. $c(10 \times 2)$ phase

With further increasing oxygen content, the next ordered phase is of $c(10 \times 2)$ periodicity. As known from another recent LEED structure determination,[4] the local coverages are $\theta^{O}_{c(10\times2)} = \theta^{Co}_{c(10\times2)} = 9/10$. The Co_4O pyramids have completely disappeared by an additional rearrangement of cobalt species as displayed in Fig. 7(d). The order in the Co layer is near hexagonal with, however, owing to the misfit with the quadratic substrate, a considerable vertical buckling (amplitude 0.50 Å), which again induces some buckling in the top two iridium layers. Also, there are considerable lateral shifts off the ideal hexagonal positions. As a consequence, two qualitatively different threefold sites for oxygen are formed. In one of them the triangle is of a smaller size than in the other, with the smaller (larger) one centered close to an iridium bridge (top) position. Oxygen forming a pyramid with the smaller triangle as a base resembles again the Co_3O pyramid in the rocksalt-type CoO(111) surface. In contrast, oxygen in the threefold site formed by the larger triangle can dive into the site so that it resides almost in plane. This degenerate Co_3O pyramid is equivalent to a local hexagonal BN-type structure, as argued in Ref. 4. The distance to the underlying Ir atom is only 2.13 Å, indicative for additional bonding of oxygen to this atom and possibly pinning that structure.

The TD spectrum for the $c(10 \times 2)$ phase starts again at lower temperatures, i.e., there must be oxygen species with even lower binding energy than discussed up to this point. Presumably, they belong to the new structural element within this phase, the degenerate BN-type Co_3O, although also oxygen bonding in the rocksalt-type pyramid should be weakened as its Co species are now all threefold coordinated to oxygen. Subsequent reordering eventually leads to the high-temperature peak, which is typical for desorption from Co_4O pyramids. For the $c(8 \times 2)$ phase the desorption spectrum is rather complex and it starts at even lower temperatures. Yet, in the absence of a quantitative structure determination, we do not speculate about the physics behind.

E. Comparison of the different phases

So far, it has been shown that with increasing oxygen content, pyramids with Co triangles as the base take over as the structural element(s). The local coverage of cobalt species as averaged over the unit cell varies only little from phase to phase, in contrast to the coverage of oxygen. The values relative to the number of atoms in the Ir layer are, for cobalt, $1 \rightarrow 8/9 \rightarrow 8/9 \rightarrow 9/10 \rightarrow 7/8$ and, for oxygen, $1/4 \rightarrow 4/9 \rightarrow 5/9 \rightarrow 9/10 \rightarrow 7/4$. The Co-Ir bond lengths appear rather unaffected by the oxidation process and vary only slightly, i.e., in the range 2.54–2.64 Å, dependent on the coordination of Co to O. Nevertheless, with progressive oxidation, the Co species more and more lose their initial high-symmetry coordination with the substrate Ir atoms and instead assume local positions determined by the respective inner-oxidic bonding configuration. The Co-O bond length is in the range 1.82–2.03 Å, again dependent on the coordination of both O (with Co) and Co (with O and Ir). In any case, the Co-O bond length is smaller than in the bulk of rocksalt-type CoO (2.13 Å). This is owing to the reduced coordination of oxygen in the various phases considered here (compared to the sixfold coordination in the bulk).

In the (2 × 2) and the two (3 × 3) phases the oxide binds to the substrate via the cobalt species only. There is even some repulsive interaction between O and Ir because the latter is pushed into the surface when lying directly below the oxygen species. In contrast, in the $c(8 \times 2)$ binding it is exclusively by oxygen, assuming the proposed O-Co-O trilayer model holds. The $c(10 \times 2)$ phase is a transition state in this sense as binding is both by cobalt (in the rocksalt-type structural element) and by the deep lying oxygen in the local BN-type structural element.

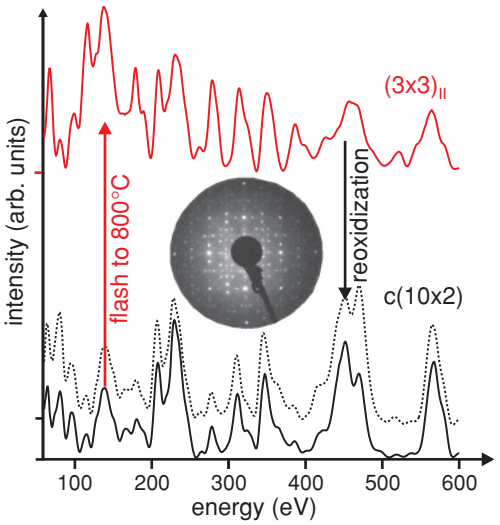

FIG. 8. (Color online) LEED spectra of the (10) beam of the $c(10 \times 2)$ phase prepared as described (full line) and of the $(3 \times 3)_{II}$ phase produced by a flash of the $c(10 \times 2)$ phase to 800 °C. By reoxidation of the $(3 \times 3)_{II}$ structure, the $c(10 \times 2)$-type spectrum presented by the broken line appears (it is slightly ofset to the first curve). The LEED pattern displayed is intermediate between both phases and exhibits a superposition of spots, representative for both. It results by an incomplete flash and cooling the sample to liquid-nitrogen temperature.

A comparison of the different TD spectra displayed in Fig. 2(a) reveals rather similar high-temperature parts for the various phases. Also, all phases can be annealed after their preparation to temperatures directly below the onset of oxygen desorption without any detectable change in the LEED appearance after cooling. This indicates that the structures retrieved are indeed stable states for the O:Co ratios given, i.e., they develop from each other under both increasing and decreasing oxygen content. As a consequence, it should be possible to prepare phases of lower oxygen content from those with higher ones via partial oxygen desorption. This is explicitly demonstrated in Fig. 8, where the $(3 \times 3)_{II}$ phase has been created simply by flashing the $c(10 \times 2)$ phase to 800 °C. Reoxidation of the latter leads, of course, again to the $c(10 \times 2)$ structure. In principle, the same holds also for the other phases. However, in practice, it turns out to be rather difficult to stop oxygen desorption at exactly the nominal coverage for the desired phase and so quite often phase mixtures result. We also want to add that by heating the $(3 \times 3)_I$ phase to reduce the oxygen content from $r_{O:Co} = 1/2$ to $r_{O:Co} = 1/4$, no long-range-ordered phase results, i.e., the structural elements typical for the (2×2) phase seem to develop only locally. Maybe the dissolution of Co into the Ir bulk already sets in at temperatures ∼1000 °C as a competing process to (2×2) reordering.

VI. CONCLUSION

In conclusion, we have observed five ordered phases in the oxidation of ∼1 ML Co deposited on Ir(100)-(1×1). The crystallography of four of them has been determined quantitatively and can be described by three structural elements. In the early stage of oxidation ($r_{O:Co} = 1/4$) this element (No. 1) is a Co_4O pyramid with a square base made up of Co and with O on top, and is arranged in (2×2) periodicity on the surface. In the next stage ($r_{O:Co} = 1/2$) part of the Co species rearrange so that Co_3O pyramids with a triangular Co base and O on top are formed as a new structural element (No. 2). This is similar to the pyramid in an oxygen-terminated (111) surface of rocksalt-type CoO films as indeed observed.[19] The other Co species remain in their quadratic arrangement whose fourfold sites are, however, not occupied. Yet they become occupied with further increasing oxygen content at $r_{O:Co} = 5/8$, so that both Co_4O and Co_3O pyramids are essential structural elements. Up to this point the bonding of the oxide to the iridium substrate is via the cobalt species. At $r_{O:Co} = 1$ the Co species in a square arrangement also rearrange to form threefold sites. This leads to the presence of two types of triangular sites in this phase. With the smaller ones again rocksalt-type pyramids (No. 2) are built. In the larger sized ones oxygen can accommodate almost in plane, thereby forming a BN-type structural element (No. 3) that can be regarded as a degenerate pyramid. This oxygen also binds to the underlying Ir atom so that this $c(10 \times 2)$ phase of the oxide is attached to the substrate via both Co and O. As indicated by TD spectra, the Co_4O pyramid appears to be the energetically most stable structural element followed by the other different Co_3O pyramids. By desorption of oxygen from a certain phase, the structural elements typical for the phases with less oxygen content are reproduced. The observed ordered phases may be a challenge for density functional theory calculations, which for cobalt oxide are additionally complicated by strong electron-electron correlations. As the crystallographic structures have been reliably determined, calculations should reproduce them as functions of the chemical potential of oxygen.

ACKNOWLEDGEMENT

The authors are grateful for financial support by Deutsche Forschungsgemeinschaft.

[1] F. P. Netzer, F. Allegretti, and S. Surnev, J. Vac. Sci. Technol. B **28**, 1 (2010).
[2] F. P. Netzer, Surf. Sci. **604**, 485 (2010).
[3] M. Gubo, C. Ebensperger, W. Meyer, L. Hammer, and K. Heinz, J. Phys. Condens. Matter **21**, 474211 (2009).
[4] C. Ebensperger, M. Gubo, W. Meyer, L. Hammer, and K. Heinz, Phys. Rev. B **81**, 235405 (2010).
[5] C. Giovanardi, L. Hammer, and K. Heinz, Phys. Rev. B **74**, 125429 (2006).
[6] J. Küppers and H. Michel, Appl. Surf. Sci. **3**, 179 (1979).
[7] K. Heinz, G. Schmidt, L. Hammer, and K. Müller, Phys. Rev. B **32**, 6214 (1985).
[8] D. Lerch, A. Klein, A. Schmidt, S. Müller, L. Hammer, K. Heinz, and M. Weinert, Phys. Rev. B **73**, 075430 (2006).
[9] K. Heinz, Rep. Prog. Phys. **58**, 637 (1995).
[10] P. J. Rous, J. B. Pendry, D. K. Saldin, K. Heinz, K. Müller, and N. Bickel, Phys. Rev. Lett. **57**, 2951 (1986).
[11] P. J. Rous and J. B. Pendry, Prog. Surf. Sci. **39**, 3 (1992).
[12] V. Blum and K. Heinz, Comput. Phys. Commun. **134**, 392 (2001).
[13] M. Kottcke and K. Heinz, Surf. Sci. **376**, 352 (1997).
[14] J. B. Pendry, J. Phys. C **13**, 937 (1980).
[15] J. Rundgren, Phys. Rev. B **68**, 125405 (2003).
[16] A. Schmidt, W. Meier, L. Hammer, and K. Heinz, J. Phys. Condens. Matter **14**, 12353 (2002).
[17] P. A. Redhead, Vacuum **12**, 203 (1962).
[18] K. Biedermann, M. Gubo, L. Hammer, and K. Heinz, J. Phys. Condens. Matter **21**, 185003 (2009).
[19] W. Meyer, K. Biedermann, M. Gubo, L. Hammer, and K. Heinz, Phys. Rev. B **79**, 121403(R) (2009).
[20] M. Gierer, H. Over, P. Rech, E. Schwarz, and K. Christmann, Surf. Sci. **370**, L201 (1997).